Figure 4 establishes that the SAP airfoil flow is generally better than that of the fixed shape 8.5 airfoil on the upstroke. The peak vorticity flux for the SAP airfoil moves slightly upstream with increasing angle of attack (from $x/c = 0.08$ to 0.05; Figs. 4b–4d), but it is lower than that for the shape 8.5 airfoil. The large peak of 225 seen for the fixed shape 8.5 airfoil close to the leading edge in Fig. 4b is not observed for the SAP airfoil, even though its instantaneous shape of 7.5 attained dynamically is very close to the fixed shape 8.5. This can be attributed to the extreme sensitivity of the flow to the dynamic change of leading-edge curvature. At $\alpha = 20$ deg (Fig. 4d), the peak vorticity in the SAP airfoil flow drops to about 50% of that seen in the fixed shape 8.5 airfoil flow, occurring at $x/c = 0.05$. In this, the peak vorticity occurs away from the leading edge and is significantly lower, when compared to the NACA 0012 airfoil before onset of dynamic stall. This explains why no dynamic stall vortex was observed in the deforming airfoil flow. On the downstroke at $\alpha = 19$ deg (Fig. 4e), the SAP airfoil flow vorticity level is somewhat higher and leads the fixed shape 8.5 airfoil, a trend that can be traced to the peak suction pressure being higher during the downstroke for the SAP airfoil. In Fig. 4f, the values for the fixed shape 8.5 airfoil are compared at $\alpha = 15.5$ deg with the SAP airfoil at $\alpha = 15$ deg. The higher vorticity flux levels suggest that a somewhat improved lift performance can be expected from the SAP airfoil due to the increased circulation due to this vorticity.

IV. Conclusions

1) Compressible dynamic stall has been successfully controlled using dynamic shape adaptation. This required a very small (0.6-mm) change in the chord length of a dynamically adaptive airfoil that produced a nearly 150% change in the leading-edge radius of curvature.

2) The flow was found to be dynamic stall vortex free for $M = 0.3$, $k = 0.05$, and $\alpha = 10 + 10 \sin \omega t$ deg. The favorable effects of dynamic shape adaptation realized through changes in the instantaneous potential flow resulted in broader pressure distributions with lower peak suction values and led to a redistribution of the unsteady flow vorticity. The vorticity levels decreased to values where the dynamic stall vortex did not form.

3) The peak suction variation loop over the oscillation cycle was found to be the smallest for the adapting airfoil.

4) The deformation rate, the initiation angle of attack, and the amount of nose curvature change affect the success of the approach significantly. The most benefit is produced while remaining within the attached flow envelope for a given Mach number during dynamic shape adaptation.

Acknowledgments

This work was supported by a Research Grant (MIPR8BNP-SARO07) from the U.S. Army Research Office and was monitored by T. L. Doligalski. The support of S. S. Davis, Fluid Mechanics Laboratory of NASA Ames Research Center, the assistance of R. A. Miller in model installation, and the control system design effort of D. D. Squires and M. Khov, Sverdrup Technology, Inc., are gratefully acknowledged.

References

[1]Chandrasekhara, M. S., Wilder, M. C., and Carr, L. W., "Unsteady Stall Control Using Dynamically Deforming Airfoils," *AIAA Journal*, Vol. 36, No. 3, 1998, pp. 1792–1800.

[2]Chandrasekhara, M. S., Carr, L. W., Wilder, M. C., Sticht, C. D., and Paulson, G. N., "Design and Development of a Dynamically Deforming Leading Edge Airfoil for Unsteady Flow Control," *ICIASF'97 RECORD*, IEEE Publication 97CH36121, Inst. of Electrical and Electronics Engineers, Piscataway, NJ, 1997, pp. 132–140.

[3]Chandrasekhara, M. S., Carr, L. W., and Wilder, M. C., "Compressible Dynamic Stall Control Using a Shape Adaptive Airfoil," AIAA Paper 99-0650, Jan. 1999.

[4]Ahmed, S., and Chandrasekhara, M. S., "Reattachment Studies of an Oscillating Airfoil Dynamic Stall Flowfield," *AIAA Journal*, Vol. 32, No. 5, 1994, pp. 1006–1012.

A. Plotkin
Associate Editor

Flexibility Equations for Active Rack Isolation System Umbilicals with Planar End Loading

R. David Hampton*
U.S. Military Academy, West Point, New York 10996
Naveed Quraishi†
NASA Johnson Space Center, Houston, Texas 77058
and
Jason K. Rupert‡
Dynetics, Inc., Huntsville, Alabama 35806

Introduction

THE Active Rack Isolation System (ARIS) serves as the central component of an integrated, station-wide strategy to isolate microgravity space-science experiments on the International Space Station (ISS). ARIS uses 8 electromechanical actuators to isolate an International Standard Payload Rack (ISPR) from disturbances due to the motion of the ISS; 11 ARIS racks are being developed for the ISS. Disturbances to microgravity experiments on ARIS-isolated racks are transmitted primarily via the (nominally 13) ARIS umbilicals, which provide power, data, vacuum, cooling, and other miscellaneous services to the experiments. The two power umbilicals and, to a lesser extent, the vacuum umbilical, serve as the primary transmission path for acceleration disturbances. Experimental tests conducted by the ARIS team[1] (December 1998) indicate that looped power umbilicals resonate at about 10 Hz; unlooped power umbilicals resonate at about 4 Hz. In either case, the ARIS controller's limited bandwidth (about 2 Hz) admits only limited active isolation at these frequencies. Reduction in the umbilical resonant frequencies could help to address this problem.

Analytical studies of the nonlinear bending and deflection of a flexible, linearly elastic, fixed-end, cantilever beam (originally horizontal) have been conducted for a variety of loading conditions, including concentrated terminal transverse (vertical) loading[2–6]; uniformly distributed vertical loading[2,7–9]; uniformly distributed normal loading[10]; concentrated terminal inclined loading[11,12]; multiple concentrated vertical loads[13]; concentrated terminal vertical and moment loading[13]; and heavy, rigid, end-attachment loading.[14] Reference 15 provided a set of nonlinear equations for the case of a weightless flexible beam, with arbitrary, discrete, in-plane loads and boundary conditions. Typical exact solutions of beam deflections involve complete and incomplete elliptic integrals (for example, Refs. 2, 4–6, 13, and 14). For literature reviews, see Refs. 16–18.

In the special case of general terminal in-plane loading, that is, including both inclined-force and moment loads, in-plane flexibility (or stiffness) equations would be of particular interest toward umbilical design for microgravity-isolation purposes. The equations could be used to help optimize umbilical flexibilities and resonant frequencies for microgravity applications.

This Note develops equations for the in-plane deflections and flexibilities of an idealized umbilical (thin, flexible, prismatic, linearly elastic, fixed-end, cantilevered, with equal tensile and compressive moduli of elasticity) under terminal in-plane loading (inclined-force and moment). The effect of gravity can be neglected due to the on-orbit application. (Note that the deflection analysis is a special case of the treatment presented in Ref. 15.) The deflection and flexibility

Received 18 September 2000; revision received 18 June 2001; accepted for publication 20 June 2001.

*Associate Professor, Department of Civil and Mechanical Engineering. Member AIAA.

†Program Manager for the Active Rack Isolation System International Space Station Characterization Experiment, Payloads Office. Member AIAA.

‡Engineer, Missile Systems Department, Simulation and Analysis Section. Member AIAA.

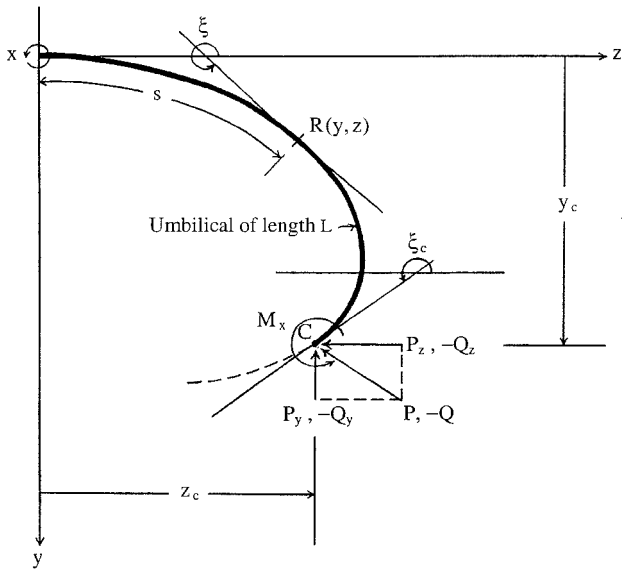

Fig. 1 Flexible umbilical under end loading.

analyses are applicable to an initially straight, cantilevered umbilical with uniform cross section, which undergoes large deflections with no plastic deformation, such that the umbilical terminus remains in a single quadrant and the umbilical slope changes monotonically. The analysis would be applicable to the ARIS power and vacuum umbilicals, under the indicated assumptions.

Problem Statement

Consider an idealized umbilical of length L with endpoints O and C and arbitrary intermediate point R (Fig. 1). Let R be located at distance s along the umbilical, measured from the cantilevered end, with coordinates (y, z); the coordinates of point C are (y_c, z_c). The coordinates have been chosen to be consistent with the coordinate system in use for the existing analyses of ARIS, for dynamic-modeling and controller-design purposes; point O, then, is the umbilical point of attachment to the ISS, and point C is the point of attachment to the ISPR. Let ξ be the angle, at R, of the tangent to the umbilical; let ξ_c represent the endpoint angle at C. Assume that ξ varies monotonically, remaining in the range $\pi \le \xi \le 2\pi$, and that the flexural rigidity EI is known.

This Note accomplishes the following fundamental tasks: 1) to (re)derive,[15] in convenient form, geometric equations for the umbilical length, coordinates at arbitrary point R, and terminal coordinates (at C) and 2) to use these equations to derive useful equations for the nine in-plane umbilical flexibilities. These 14 equations will be expressed in terms of the angle ξ_c and of the in-plane loads at C. The loads are as follows: forces Q_y and Q_z, in the positive y and z directions, respectively, and counterclockwise (positive) moment M_x about the positive x axis.

Equations of Umbilical Geometry

At point R the moment equation is

$$M = EI\frac{\mathrm{d}\xi}{\mathrm{d}s} = M_x + Q_z(y_c - y) - Q_y(z_c - z) \tag{1}$$

Differentiating with respect to s, observing that

$$\frac{\mathrm{d}y}{\mathrm{d}s} = -\sin\xi \tag{2}$$

$$\frac{\mathrm{d}z}{\mathrm{d}s} = \cos\xi \tag{3}$$

and using the shorthand notation, $s_\xi = \sin\xi$ and $c_\xi = \cos\xi$, one obtains

$$\frac{\mathrm{d}^2\xi}{\mathrm{d}s^2} = \frac{Q_z}{EI}s_\xi + \frac{Q_y}{EI}c_\xi \tag{4}$$

Integrating Eq. (4) with respect to s yields

$$\frac{1}{2}\left(\frac{\mathrm{d}\xi}{\mathrm{d}s}\right)^2 = \frac{1}{EI}(Q_y s_\xi - Q_z c_\xi) + C_1 \tag{5}$$

where C_1 is an integration constant. At point C, Eq. (1) becomes

$$M_x = EI\left.\frac{\mathrm{d}\xi}{\mathrm{d}s}\right|_{R\to C} \tag{6}$$

Applying this boundary condition to Eq. (5), one has

$$C_1 = \tfrac{1}{2}(M_x/EI)^2 - (1/EI)\left(Q_y s_{\xi_c} - Q_z c_{\xi_c}\right) \tag{7}$$

so that Eq. (5) can now be solved for $\mathrm{d}\xi/\mathrm{d}s$:

$$\frac{\mathrm{d}\xi}{\mathrm{d}s} = -\left\{\frac{2}{EI}\left[Q_y\left(s_\xi - s_{\xi_c}\right) - Q_z\left(c_\xi - c_{\xi_c}\right)\right] + \left(\frac{M_x}{EI}\right)^2\right\}^{\frac{1}{2}} = -\eta^{\frac{1}{2}} \tag{8}$$

where the radicand

$$\eta \equiv (2Q_y/EI)\left(s_\xi - s_{\xi_c}\right) - (2Q_z/EI)\left(c_\xi - c_{\xi_c}\right) + (M_x/EI)^2 \tag{9}$$

Equation (8) applies under the assumption that the radicand η is nonnegative, or, equivalently, that $\mathrm{d}\xi/\mathrm{d}s$ is nonpositive.

From Eq. (8),

$$\mathrm{d}s = -\eta^{-\frac{1}{2}}\,\mathrm{d}\xi \tag{10}$$

which can be integrated to yield an expression for the umbilical length:

$$L = \int_0^L \mathrm{d}s = \int_{2\pi}^{\xi_c} -\eta^{-\frac{1}{2}}\,\mathrm{d}\xi = \int_{\xi_c}^{2\pi} \eta^{-\frac{1}{2}}\,\mathrm{d}\xi \tag{11}$$

From Eq. (2),

$$\mathrm{d}y = s_\xi \eta^{-\frac{1}{2}}\,\mathrm{d}\xi \tag{12}$$

so that

$$y = -\int_\xi^{2\pi} \eta^{-\frac{1}{2}} s_\xi\,\mathrm{d}\xi \tag{13}$$

$$y_c = -\int_{\xi_c}^{2\pi} \eta^{-\frac{1}{2}} s_\xi\,\mathrm{d}\xi \tag{14}$$

Likewise, Eq. (3) yields

$$z = \int_\xi^{2\pi} \eta^{-\frac{1}{2}} c_\xi\,\mathrm{d}\xi \tag{15}$$

$$z_c = \int_{\xi_c}^{2\pi} \eta^{-\frac{1}{2}} c_\xi\,\mathrm{d}\xi \tag{16}$$

Together, Eqs. (11) and (13–16) describe the umbilical geometry as functions of the terminal angle ξ_c; terminal loads Q_y, Q_z, and M_x; and integration or shape kernel η.

As a check of the mathematics, one can show straightforwardly that for the case of a horizontal cantilever with a vertical point load at the free end, that is, for Q_y and M_x both zero, Eq. (11) simplifies to the following:

$$L = (1/k)K(p) \tag{17}$$

where

$$k^2 = \frac{P_z}{EI} \tag{18}$$

$$K(p) = F\left(p, \frac{\pi}{2}\right) = \int_0^{\pi/2} (1 - p^2\sin^2\varsigma)^{-\frac{1}{2}}\,\mathrm{d}\varsigma \tag{19}$$

$K(p)$ and $F(p, \phi)$, respectively, are Legendre's complete and incomplete elliptic integrals of the first kind.[13]

For the case of a horizontal cantilever with a horizontal point load at the free end, that is, for Q_z and M_x both zero, Eq. (11) simplifies to the following:

$$L = (EI/Q_y)^{\frac{1}{2}}[K(p) - F(p, m)] \tag{20}$$

where

$$m = \sin^{-1}\left(1\Big/p\sqrt{2}\right) \tag{21}$$

Equation (20) is the solution previously reported in Ref. 13.

Equations of Umbilical Flexibility

Nature of Dependencies on Flexural Rigidity *EI*

It will now be shown that, for constant values of L, ξ_c, y_c, and z_c, that is, umbilical length and terminal geometry, the following expressions are also constants: Q_y/EI, Q_z/EI, and M_x/EI. This will have important implications for umbilical shapes and flexibilities.

Consider two umbilicals ($i = 1, 2$) of uniform cross section, for which (as before) the respective tangent angles ξ_i vary monotonically in the range $\pi \le \xi_i \le 2\pi$. Assume also that the umbilicals have identical lengths and terminal geometries but different flexural rigidities and, in consequence, different (nonzero) terminal loads. In particular,

$$L_1 = L_2 \tag{22}$$

$$y_{c1} = y_{c2} \tag{23}$$

$$z_{c1} = z_{c2} \tag{24}$$

$$\xi_{c1} = \xi_{c2} \tag{25}$$

where

$$L_i = \int_{\xi_c}^{2\pi} \eta_i^{-\frac{1}{2}}\,\mathrm{d}\xi > 0 \tag{26}$$

$$y_{ci} = -\int_{\xi_c}^{2\pi} \eta_i^{-\frac{1}{2}} s_\xi\,\mathrm{d}\xi > 0 \tag{27}$$

$$z_{ci} = \int_{\xi_c}^{2\pi} \eta_i^{-\frac{1}{2}} c_\xi\,\mathrm{d}\xi > 0 \tag{28}$$

for

$$\eta_i = \eta_i(\xi) \equiv \frac{2Q_{yi}}{(EI)_i}\left(s_\xi - s_{\xi_c}\right) - \frac{2Q_{zi}}{(EI)_i}\left(c_\xi - c_{\xi_c}\right) + \left(\frac{M_{xi}}{(EI)_i}\right)^2 \ge 0 \tag{29}$$

For simplicity, define the following:

$$\alpha_{1i} = Q_{yi}/(EI)_i \tag{30}$$

$$\alpha_{2i} = Q_{zi}/(EI)_i \tag{31}$$

$$\alpha_{3i} = M_{xi}/(EI)_i \tag{32}$$

so that

$$\eta_i = 2\alpha_{1i}\left(s_\xi - s_{\xi_c}\right) - 2\alpha_{2i}\left(c_\xi - c_{\xi_c}\right) + \alpha_{3i}^2 \tag{33}$$

With Eqs. (26–28), Eqs. (22–24) can be rewritten, respectively, as follows:

$$L_1 = \int_{\xi_c}^{2\pi} \eta_1^{-\frac{1}{2}}\,\mathrm{d}\xi = \int_{\xi_c}^{2\pi} \eta_2^{-\frac{1}{2}}\,\mathrm{d}\xi = L_2 \tag{34}$$

$$y_{c1} = -\int_{\xi_c}^{2\pi} \eta_1^{-\frac{1}{2}} s_\xi\,\mathrm{d}\xi = -\int_{\xi_c}^{2\pi} \eta_2^{-\frac{1}{2}} s_\xi\,\mathrm{d}\xi = y_{c2} \tag{35}$$

$$z_{c1} = \int_{\xi_c}^{2\pi} \eta_1^{-\frac{1}{2}} c_\xi\,\mathrm{d}\xi = \int_{\xi_c}^{2\pi} \eta_2^{-\frac{1}{2}} c_\xi\,\mathrm{d}\xi = z_{c2} \tag{36}$$

From the orthogonality of the constant (unity), sine, and cosine functions in Eqs. (34–36), respectively, it follows that

$$\sqrt{\eta_1} = \sqrt{\eta_2} \tag{37}$$

That is, with uniform cross sections and identical umbilical attachment angles,

$$\left.\begin{aligned} L_1 &= L_2 \\ y_{c1} &= y_{c2} \\ z_{c1} &= z_{c2} \end{aligned}\right\} \Rightarrow \sqrt{\eta_1} = \sqrt{\eta_2} \tag{38}$$

It can be shown trivially (by simple substitution) that the only if statement of Eq. (38) is, in fact, if and only if ($\Leftrightarrow$).

Using Eq. (33), one can rewrite Eq. (37) as follows:

$$\sqrt{\eta_1} = \sqrt{2\alpha_{11}\left(s_\xi - s_{\xi_c}\right) + 2\alpha_{21}\left(c_\xi - c_{\xi_c}\right) + \alpha_{31}^2}$$

$$= \sqrt{2\alpha_{12}\left(s_\xi - s_{\xi_c}\right) + 2\alpha_{22}\left(c_\xi - c_{\xi_c}\right) + \alpha_{32}^2} = \sqrt{\eta_2} \tag{39}$$

Squaring and applying orthogonality as before, one concludes readily that Eq. (39) holds only if ($\Rightarrow$) the following are true:

$$\alpha_{11} = \alpha_{12} \tag{40}$$

$$\alpha_{21} = \alpha_{22} \tag{41}$$

$$\alpha_{31}^2 = \alpha_{32}^2 \tag{42}$$

Again, it can be shown trivially that this relationship is actually if and only if.

Equation (1), evaluated at point C, leads to the conclusion that $M_x \le 0$. With Eqs. (32) and (37) (again, evaluated at point C) this leads to the following:

$$\sqrt{\eta_1} = -\alpha_{31} = -\alpha_{32} = \sqrt{\eta_2} \tag{43}$$

In summary, it has been shown that, for two slender umbilicals ($i = 1, 2$) with 1) uniform cross sections, 2) identical umbilical attachment angles, 3) umbilicals and umbilical termini remaining in a single quadrant, and 4) respective umbilical slopes changing monotonically,

$$\left.\begin{aligned} L_1 &= L_2 \\ y_{c1} &= y_{c2} \\ z_{c1} &= z_{c2} \end{aligned}\right\} \Leftrightarrow \sqrt{\eta_1} = \sqrt{\eta_2} \Leftrightarrow \begin{cases} \left(\dfrac{Q_y}{EI}\right)_1 = \left(\dfrac{Q_y}{EI}\right)_2 \\ \left(\dfrac{Q_z}{EI}\right)_1 = \left(\dfrac{Q_z}{EI}\right)_2 \\ \left(\dfrac{M_x}{EI}\right)_1 = \left(\dfrac{M_x}{EI}\right)_2 \end{cases} \tag{44}$$

Because, then, for fixed umbilical length and geometry Q_y/EI, Q_z/EI, and M_x/EI are constants, changing the flexural rigidity by some factor γ changes all of the terminal loads by the same factor; however, the umbilical shape will remain unchanged [Eqs. (13) and (15)]. The implications for in-plane umbilical stiffnesses will be explored in the next section.

Basic Flexibility Equations

For given terminal geometry (ξ_c, y_c, and z_c), Leibnitz's rule can now be applied to Eqs. (11), (14), and (16) to yield expressions for the nine in-plane translational flexibilities. For convenience, define the following normalized loads and flexibility integrals:

$$\alpha_1 = \frac{Q_y}{EI} \tag{45}$$

$$\alpha_2 = \frac{Q_z}{EI} \tag{46}$$

$$\alpha_3 = \frac{-M_x}{EI} \tag{47}$$

$$\alpha_4 = \frac{\mu}{EI} = c_{\xi_c}\alpha_1 + s_{\xi_c}\alpha_2 \tag{48}$$

$$\beta_1 = \int_{\xi_c}^{2\pi} \eta^{-\frac{3}{2}}\,\mathrm{d}\xi \tag{49}$$

$$\beta_2 = \int_{\xi_c}^{2\pi} \eta^{-\frac{3}{2}} c_\xi \, \mathrm{d}\xi \tag{50}$$

$$\beta_3 = \int_{\xi_c}^{2\pi} \eta^{-\frac{3}{2}} s_\xi \, \mathrm{d}\xi \tag{51}$$

$$\beta_4 = \int_{\xi_c}^{2\pi} \eta^{-\frac{3}{2}} c_\xi^2 \, \mathrm{d}\xi \tag{52}$$

$$\beta_5 = \int_{\xi_c}^{2\pi} \eta^{-\frac{3}{2}} c_\xi s_\xi \, \mathrm{d}\xi \tag{53}$$

$$\beta_6 = \int_{\xi_c}^{2\pi} \eta^{-\frac{3}{2}} s_\xi^2 \, \mathrm{d}\xi \tag{54}$$

where

$$\eta = 2\alpha_1\left(s_\xi - s_{\xi_c}\right) - 2\alpha_2\left(c_\xi - c_{\xi_c}\right) + \alpha_3^2 \tag{55}$$

With these symbols, the nine in-plane flexibility equations are as follows:

$$\frac{\partial y_c}{\partial Q_y} = \frac{1}{EI}\left[\left(\beta_6 - s_{\xi_c}\beta_3\right) - \left(\beta_3 - s_{\xi_c}\beta_1\right)\left(\frac{s_{\xi_c} + \alpha_3\alpha_4\beta_3}{1 + \alpha_3\alpha_4\beta_1}\right)\right] \tag{56}$$

$$\frac{\partial y_c}{\partial Q_z} = \frac{-1}{EI}\left[\left(\beta_5 - c_{\xi_c}\beta_3\right) - \left(\beta_2 - c_{\xi_c}\beta_1\right)\left(\frac{s_{\xi_c} + \alpha_3\alpha_4\beta_3}{1 + \alpha_3\alpha_4\beta_1}\right)\right] \tag{57}$$

$$\frac{\partial y_c}{\partial M_x} = \frac{-\alpha_3}{EI}\left[\beta_3 - \beta_1\left(\frac{s_{\xi_c} + \alpha_3\alpha_4\beta_3}{1 + \alpha_3\alpha_4\beta_1}\right)\right] \tag{58}$$

$$\frac{\partial z_c}{\partial Q_y} = \frac{-1}{EI}\left[\left(\beta_5 - s_{\xi_c}\beta_2\right) - \left(\beta_3 - s_{\xi_c}\beta_1\right)\left(\frac{c_{\xi_c} + \alpha_3\alpha_4\beta_2}{1 + \alpha_3\alpha_4\beta_1}\right)\right] \tag{59}$$

$$\frac{\partial z_c}{\partial Q_z} = \frac{1}{EI}\left[\left(\beta_4 - c_{\xi_c}\beta_2\right) - \left(\beta_2 - c_{\xi_c}\beta_1\right)\left(\frac{c_{\xi_c} + \alpha_3\alpha_4\beta_2}{1 + \alpha_3\alpha_4\beta_1}\right)\right] \tag{60}$$

$$\frac{\partial z_c}{\partial M_x} = \frac{\alpha_3}{EI}\left[\beta_2 - \beta_1\left(\frac{c_{\xi_c} + \alpha_3\alpha_4\beta_2}{1 + \alpha_3\alpha_4\beta_1}\right)\right] \tag{61}$$

$$\frac{\partial \xi_c}{\partial Q_y} = \frac{\alpha_3}{EI}\left[\frac{\beta_3 - s_{\xi_c}\beta_1}{1 + \alpha_3\alpha_4\beta_1}\right] \tag{62}$$

$$\frac{\partial \xi_c}{\partial Q_z} = \frac{-\alpha_3}{EI}\left[\frac{\beta_2 - c_{\xi_c}\beta_1}{1 + \alpha_3\alpha_4\beta_1}\right] \tag{63}$$

$$\frac{\partial \xi_c}{\partial M_x} = \frac{\alpha_3^2}{EI}\left[\frac{-\beta_1}{1 + \alpha_3\alpha_4\beta_1}\right] \tag{64}$$

where α_3 and the square-bracketed expressions are all invariant with EI. This means physically that changing the flexural rigidity by some factor γ changes all of the in-plane stiffnesses by the same factor.

Implications for Umbilical Design

The foregoing equations can be used as an aid for designing umbilicals to minimize stiffness. First, from Eqs. (44) and (56–64), one sees that reductions in flexural rigidity will produce proportional reductions in all terminal loads and in-plane stiffnesses. Second, for given umbilical length L and endpoint conditions ξ_c, z_c, and y_c, Eqs. (11), (14), and (16) can be solved for the loads Q_y, Q_z, and M_x. These loads can be determined and used iteratively in Eqs. (56–64) to maximize umbilical flexibilities (or, equivalently, to minimize the corresponding stiffnesses) using L as a parameter. Third, the umbilical designer can use the preceding equations to determine optimal L, ξ_c combinations. Although the angle ξ_c is fixed at about 225 deg for ARIS (in the home, or centered, position), L and ξ_c optimization could suggest better angles for future designs.

Conclusions

This Note has presented equations for the shape and flexibilities of an umbilical on orbit, that is, such that gravity can be neglected, under general, terminal, in-plane loading conditions of sufficient magnitude to cause large deformations. The umbilical was assumed to be initially straight, to have a uniform cross section, and to undergo no plastic deformation. All in-plane stiffnesses were shown to be proportional to the flexural rigidity EI. An approach was offered for using umbilical length and terminal geometry (endpoint locations and slopes) to optimize these umbilical stiffnesses. The basic equations were observed to reduce to known results for special loading conditions.

For many umblicals the assumption that the preloaded shape follows a curved, rather than straight-line, segment is more realistic. An analysis for such cases should incorporate the prebent umbilical curvature as an optimization parameter, in addition to the length and terminal geometry.

Acknowledgments

The authors are grateful to NASA Johnson Space Center for funding this work, through the 2000 NASA/American Society for Engineering Education Summer Faculty Fellowship Program.

References

[1] Edberg, D. L., and Wilson, B. W., "Design and Testing of Reduced-Stiffness Umbilicals for Space Station Microgravity Isolation," AIAA Paper 2000-1408, April 2000.

[2] Hummel, F. H., and Morton, W. B., "On the Large Deflection of Thin Flexible Strips and the Measurement of Their Elasticity," *Philosophical Magazine*, Ser. 7, Vol. 17, 1927, pp. 348–357.

[3] Gross, S., and Lehr, E., *Die Federn*, V. D. I. Verlag, Berlin, 1938.

[4] Barten, H. J., "On the Deflection of a Cantilever Beam," *Quarterly of Applied Mathematics*, Vol. 2, No. 2, 1944, pp. 168–171.

[5] Barten, H. J., "On the Deflection of a Cantilever Beam," *Quarterly of Applied Mathematics*, Vol. 3, No. 3, 1945, pp. 275, 276.

[6] Bisshopp, K. E., and Drucker, D. C., "Large Deflections of Cantilever Beams," *Quarterly of Applied Mathematics*, Vol. 3, No. 3, 1945, pp. 272–275.

[7] Bickley, W. G., "The Heavy Elastica," *Philosophical Magazine*, Ser. 7, Vol. 17, 1934, pp. 603–622.

[8] Rohde, F. V., "Large Deflections of a Cantilever Beam with a Uniformly Distributed Load," *Quarterly of Applied Mathematics*, Vol. 11, 1953, pp. 337, 338.

[9] Schmidt, R., and Dadeppo, D. A., "Large Deflections of Heavy Cantilever Beams and Columns," *Quarterly of Applied Mathematics*, Oct. 1970, pp. 441–444.

[10] Mitchell, T. P., "The Non-Linear Bending of Thin Rods," *Journal of Applied Mechanics*, Vol. 26, 1959, pp. 40–43.

[11] Beth, R. A., and Wells, C. P., "Finite Deflections of a Cantilever Strut," *Journal of Applied Physics*, Vol. 22, 1951, pp. 742–746.

[12] Massoud, M. F., "On the Problem of Large Deflection of a Cantilever Beam," *International Journal of Mechanical Sciences*, Vol. 8, Feb. 1966, pp. 141–143.

[13] Frisch-Fay, R., *Flexible Bars*, Butterworths, London, 1962, pp. 5, 42.

[14] Antman, S. S., Marlow, R. S., and Vlahacos, C. P., "The Complicated Dynamics of Heavy Rigid Bodies Attached to Deformable Rods," *Quarterly of Applied Mathematics*, Vol. 56, No. 3, 1998, pp. 431–460.

[15] Manuel, F. S., and Lee, S. L., "Flexible Bars Subjected to Arbitrary Discrete Loads and Boundary Conditions," *Journal of the Franklin Institute*, Vol. 285, No. 6, 1968, pp. 452–474.

[16] Rojahn, C., "Large Deflections of Elastic Beams," Degree of Engineer Thesis, Stanford Univ., Stanford, CA, June 1968.

[17] Gorski, W., "A Review of the Literature and a Bibliography on Finite Elastic Deflections of Bars," *Institute of Engineers, Australia: Civil Engineering Transactions*, Vol. CE18, 1976, pp. 74–85.

[18] Libai, A., and Simmonds, J. G., *The Nonlinear Theory of Elastic Shells*, 2nd ed., Cambridge Univ. Press, Cambridge, England, U.K., 1998.

A. N. Palazotto
Associate Editor